

# Strontium-89 Therapy: Measurement of Absorbed Dose to Skeletal Metastases

Glen M. Blake, Maureen A. Zivanovic, Richard M. Blaquiere, David R. Fine,  
Alexander J. McEwan, and Duncan M. Ackery

*Wessex Regional Department of Nuclear Medicine, and Wessex Body Scanner Unit,  
Southampton General Hospital, Southampton, UK; and Department of Nuclear Medicine, The  
Cross Cancer Institute, Edmonton, Alberta, Canada*

We report measurements of absorbed dose to vertebral metastases in ten patients referred for  $^{89}\text{Sr}$  therapy for disseminated prostatic carcinoma. Patients received a tracer dose of  $^{89}\text{Sr}$  at the time of  $^{89}\text{Sr}$  treatment and metastatic strontium retention was monitored scintigraphically for 6 mo. Metastatic  $^{89}\text{Sr}$  activity corrected for tissue attenuation was measured using the conjugate view principle, with special care taken to eliminate errors due to the selection of the metastatic region of interest. Metastatic volume was determined from high resolution CT images, and density inferred from Hounsfield number using the QCT bone mineral calibration of Genant and Cann. The mean absorbed dose was 850 rad/mCi (23 cGy/MBq) with a range from 220 - 2260 rad/mCi (6 to 61 cGy/MBq). The wide range found was consistent with the variation expected to arise due to differences in strontium renal plasma clearance (range 0.1–11.8 l/day) and extent of skeletal metastatic disease (varying from two small metastases to a superscan on  $[^{99m}\text{Tc}]MDP$  images) among the patients studied.

J Nucl Med 29:549–557, 1988

Palliation of bone pain associated with disseminated prostatic carcinoma remains a serious problem in the patient who has exhausted conventional therapies. Following earlier studies by Pecher (1) and Firusian (2), several groups are investigating the use of the beta-emitting radionuclide strontium-89 ( $^{89}\text{Sr}$ ) administered as an intravenous injection of strontium chloride (3–5). At the treatment activities used in these studies, haematological toxicity is minimal, and quality of life for the patient is improved if dependence on analgesic medication can be reduced.

Little is known about the absorbed dose to skeletal metastases achieved following radiostrontium therapy, although data on tumor dose are important for interpretation of clinical findings and comparison with alternative radionuclide therapies (6–8). As part of a multicenter clinical trial of  $^{89}\text{Sr}$  therapy (9), we are undertaking quantitative studies to determine, as directly and accurately as possible, by noninvasive means, the absorbed dose delivered to bone metastases. The purpose of this report is to describe the method we developed to measure metastatic dose and to present

the findings, with estimates of likely errors, in the first ten patients studied.

## METHOD

### Selection of Patients for Dosimetric Study

The patients described in this report were treated during the course of a clinical trial to evaluate  $^{89}\text{Sr}$  therapy over a range of treatment activities (5,9). All had histologically proven carcinoma of the prostate with skeletal metastases demonstrated on radiographs and technetium-99m methylene diphosphonate ( $[^{99m}\text{Tc}]MDP$ ) bone images. They were referred for radiostrontium treatment following the failure of conventional systemic therapies to control bone pain. All patients had  $[^{99m}\text{Tc}]MDP$  bone scintigraphy performed during the week preceding therapy and only those judged to have metastases suitable for accurate dosimetry were asked to take part in the quantitative studies described here. Selection of metastases was restricted to those located in the lower dorsal or lumbar spine which appeared to uniformly involve the entire body of a vertebra. The patients chosen either had isolated vertebral metastases or had diffuse metastatic disease with uniform involvement of the lower dorsal and lumbar spine. In these latter patients the lumbar vertebra L1 was selected for study.

Patients received a therapeutic dose of  $^{89}\text{Sr}$  of either 40, 60 or 80  $\mu\text{Ci}/\text{kg}$  (1.48, 2.22, or 2.96 MBq/kg) body weight, together with 1 mCi (37 MBq) of  $^{85}\text{Sr}$  chloride. The gamma

Received Mar. 12, 1987; revision accepted Sept. 28, 1987.

For reprints contact: G. M. Blake, PhD, Wessex Regional Dept. of Nuclear Medicine, Southampton General Hospital, Tremona Rd., Southampton SO9 4XY, England.

emission of  $^{85}\text{Sr}$  and the similar half-life to  $^{89}\text{Sr}$  (64.8 days compared with 50.5 days) made it a suitable tracer for imaging the kinetics of the  $^{89}\text{Sr}$  therapy dose. The two strontium nuclides were administered simultaneously via a peripheral vein with a constant infusion rate over a 1-min interval. Syringes were measured in an isotope assay calibrator before and after injection to determine accurately the administered activities. All patients performed a 24-hr urine collection which was assayed for  $^{85}\text{Sr}$  activity and combined with a measurement of plasma  $^{85}\text{Sr}$  concentration to find the renal strontium plasma clearance (10).

### Strontium-85 Scintigraphy

Metastatic retention of strontium was studied by quantifying  $^{85}\text{Sr}$  uptake using a gamma camera equipped with a high-energy collimator rated to 511 keV, with images acquired using a 20-percent window centered on the 514-keV photopeak. Posterior view images of the lumbar and lower dorsal spine of 5 min duration were recorded on a nuclear medicine computer system at 1 day and at 2, 4, 6, 8, 12, and 26 wk after treatment. Each patient image was followed by an image of a  $^{85}\text{Sr}$  flood source placed in contact with the 511-keV collimator. At the 4-wk imaging session a conjugate view study was performed (11-13) and the following additional images acquired: (a) an anterior view of the metastasis; (b) a transmission image of a standard  $^{85}\text{Sr}$  source of known activity viewed through the spine and body at the level of the metastasis. The anterior image was subtracted from this latter to obtain an image of the transmission source alone; (c) an image of the standard source on the face of the collimator. The standard used for these latter images was a 2-cm-diameter disk with an activity of ~0.3 mCi (10 MBq).

To examine the difficulties in the accurate quantification of metastatic  $^{85}\text{Sr}$  uptake due to septal penetration and scatter, a number of phantom metastases were made by soaking rectangular pieces of filter paper in  $^{85}\text{Sr}$  strontium chloride solution. The sizes chosen ranged between 3.7 cm  $\times$  2.0 cm and 5.0 cm  $\times$  3.0 cm. To reproduce the conditions of septal penetration and scatter in *in vivo* studies, the phantom metastases were imaged sandwiched between layers of the tissue equivalent material Mix D (14) at a depth of 8 cm below one surface to represent the posterior view, and 20 cm below the opposite surface to represent the anterior view. Conjugate view studies of the phantom metastases were performed in an identical manner to the patient studies, including transmission and standard source images. In this case, however, the errors can be investigated because phantom metastases and the transmission standard can be directly compared in an isotope assay calibrator.

### Quantitative Analysis of $^{85}\text{Sr}$ Images

The set of posterior view images acquired for each patient were analyzed to find  $^{85}\text{Sr}$  counts in a rectangular region of interest (ROI) drawn to encompass the selected metastasis at a contour level of ~20% of peak metastatic count rate above local background. The same ROI was superimposed on successive images in the set, using a region shifting routine to allow for small differences in patient positioning. In a similar manner, a ROI of constant size was superimposed on the flood source images, and counts in the latter used to correct patient counts for radioactive decay and small variations in gamma camera sensitivity. The metastatic retention function

thus found was normalized to give strontium uptake as a percentage of injected dose from an analysis of the conjugate view images using a method which we now describe. The aim was to obtain an accurate estimate of strontium retention that was independent of the size of the ROI drawn round the metastasis.

We consider first the case of an isolated metastasis uniformly involving the body of a lumbar or lower dorsal vertebra, with the remainder of the spine in the field of view uninvolved (Fig. 1A). Let  $N_{\text{post}}(A)$  be the count rate recorded on the posterior conjugate view image in a rectangular ROI of area  $A \text{ cm}^2$  centered on the metastasis. When the same ROI is superimposed on the anterior, transmission and standard source images, we obtain count rates  $N_{\text{ant}}(A)$ ,  $N_{\text{trans}}(A)$ , and  $N_{\text{std}}(A)$ , respectively. We consider a set of areas, each increasing by 2 pixels in width and height (Fig. 1A).

A difficulty with accurate quantification of metastatic strontium retention is that, due to the finite point response function of the gamma camera, the image of the metastasis is larger than its true physical size. If  $A$  is made only as large as the physical size of the metastasis, not all counts due to metastatic  $^{85}\text{Sr}$  activity are included within the ROI. However, if  $A$  is made larger, there will be a significant contribution from counts from adjacent normal vertebrae. To overcome this problem, the set of ROIs was superimposed on an area of normal bone 10 cm away from the chosen metastasis, and count rates for normal bone,  $B_{\text{post}}(A)$  and  $B_{\text{ant}}(A)$ , subtracted from those for the metastasis, giving a set of corrected counts:

$$\begin{aligned} \tilde{N}_{\text{post}}(A) &= N_{\text{post}}(A) - B_{\text{post}}(A) \\ \tilde{N}_{\text{ant}}(A) &= N_{\text{ant}}(A) - B_{\text{ant}}(A) \end{aligned} \quad (1)$$

However, by making this correction we subtract not only the counts in  $A$  arising from normal bone but also a normal vertebral count level from the metastasis itself. The activity inferred from  $\tilde{N}_{\text{post}}(A)$  and  $\tilde{N}_{\text{ant}}(A)$  using the conjugate view principle will therefore be the metastatic activity in excess of that present in a normal vertebra and will require correction by a factor:

$$f_i = \frac{\text{metastatic activity}}{\text{metastatic activity} - \text{normal vertebral activity}}. \quad (2)$$

An estimate of  $f_i$  was obtained by examining the vertical profile of  $^{85}\text{Sr}$  activity along the length of the spine (Fig. 2). The profile was obtained from the patient's posterior conjugate view image by summing pixel counts in successive horizontal strips between two vertical lines drawn 5 cm apart down either edge of the spine. The shaded area of Fig. 2A (net counts  $N_M$ ) represents the metastatic count after subtraction of the background level derived from adjacent normal bone [Eq. (1)]. The shaded area of Figure 2B (net counts  $N_V$ ), defined by the product of the mean counts/cm over normal bone and the vertical height of a single vertebra (a typical vertebral height of 3 cm was determined from lateral CT scout images), represents the normal vertebral count. It follows from Eq. (2) that:

$$f_i = \frac{N_M + N_V}{N_M} \quad (3)$$

The count rate  $\tilde{N}_{\text{post}}(A)$  [Eq (1)] increases with  $A$  (Fig. 3A), emphasizing the difficulty in determining true metastatic count rate due to septal penetration and scatter. This problem

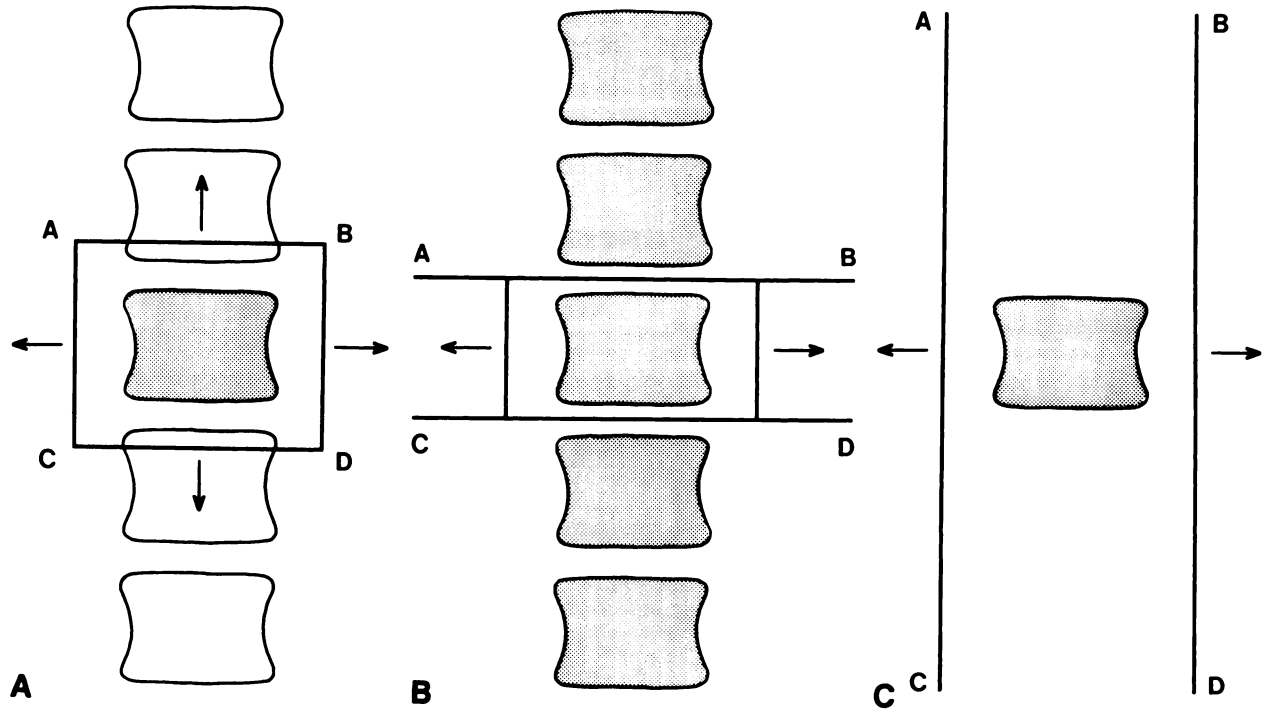


**FIGURE 1**

A: Regions of interest (ROIs) drawn for the quantification of  $^{85}\text{Sr}$  retention in an isolated vertebral metastasis (hatched area in figure). A set of rectangular ROIs was drawn each increasing in size by two pixels in width and two in height. B: ROIs drawn for the quantification of vertebral  $^{85}\text{Sr}$  retention in a patient with diffuse metastatic disease. A set of rectangular ROIs was drawn each increasing by two pixels in width. C:  $^{85}\text{Sr}$  counts in the ROIs of Figure 1B are equal to the counts obtained for a hypothetical isolated single vertebra when the latter is analyzed with the ROIs shown here. For patients with diffuse metastatic disease, anterior and posterior images were analyzed with the ROIs shown in Figure 1B and transmission and standard source images with the ROIs shown here.

is partially overcome when the conjugate view principle is applied. Let  $J_{\text{met}}(A)$  be the apparent  $^{85}\text{Sr}$  activity in the metastasis determined from the conjugate view method when a region of area  $A$  is used, and let  $J_{\text{std}}$  be the activity in the standard source. We may write (11–13):

$$J_{\text{met}}(A) = J_{\text{std}} f_1 f_2 F_{\text{met}}(A) \quad (4)$$

where:

$$F_{\text{met}}(A) = \left\{ \frac{\tilde{N}_{\text{post}}(A) \tilde{N}_{\text{ant}}(A)}{N_{\text{std}}(A) N_{\text{trans}}(A)} \right\}^{1/2}, \quad (5)$$

$f_1$  is the correction factor of Eq. (3) and  $f_2$  is a term dependent on the finite distribution of activity in the metastasis along the anterior-posterior axis. For a uniform slab source of thickness  $d$ , mass attenuation coefficient  $\mu_m$  and density  $\rho$  there is a well known relation (11–13):

$$f_2 = \frac{d \mu_m \rho / 2}{\sinh(d \mu_m \rho / 2)}. \quad (6)$$

A rough estimate of  $f_2$  may be obtained from Eq. (6) by using the approximate values  $d \sim 5 \text{ cm}$ ,  $\mu_m \sim 0.1 \text{ cm}^2/\text{g}$  and  $\rho \sim 1.4 \text{ g/cm}^3$ , giving  $f_2 \sim 0.98$ . A more rigorous calculation was obtained from an analysis of the high resolution CT images used in the estimation of metastatic mass, and this is discussed in Appendix 1.

The limitation of using Eq. (4) to measure metastatic uptake is that, due to the finite distribution of activity in the image plane,  $J_{\text{met}}(A)$  varies with  $A$  (Fig. 3B). To remove the remain-

ing uncertainty in the determination of metastatic strontium retention we write:

$$J_{\text{met}}(A) = f_{\text{met}}(A) J_{\text{met}}, \quad (7)$$

where  $J_{\text{met}}$  is the true metastatic  $^{85}\text{Sr}$  activity and  $f_{\text{met}}(A)$  an area dependent error factor. The error factor  $f_{\text{met}}(A)$  was evaluated from a study of the conjugate view images of the phantom metastases. By analogy with Eqs. (4) and (7) we may write for the conjugate view analysis of a phantom metastasis:

$$\begin{aligned} J_{\text{phant}}(A) &= J_{\text{std}} F_{\text{phant}}(A) \\ J_{\text{phant}}(A) &= f_{\text{phant}}(A) J_{\text{phant}} \end{aligned} \quad (8)$$

The phantom that most closely represented the distribution of activity in the patient's metastasis was found by matching the distribution  $F_{\text{met}}(A)$  to the set of functions  $F_{\text{phant}}(A)$  determined for the phantom metastases. When  $F_{\text{met}}(A)$  and  $F_{\text{phant}}(A)$  scale in a similar manner with  $A$ , the size of the phantom matches that of the metastasis and we may write:

$$f_{\text{phant}}(A) = f_{\text{met}}(A). \quad (9)$$

Eqs. (4), (7), (8) and (9) may be solved to give:

$$J_{\text{met}} = J_{\text{phant}} f_1 f_2 F_{\text{met}}(A) / F_{\text{phant}}(A). \quad (10)$$

When the correct phantom size is chosen, different choices of  $A$  give the same estimate of true metastatic activity. This is shown in Figure 3C, where the different estimates are plotted against  $A$  and shown not to vary by more than the statistical accuracy.

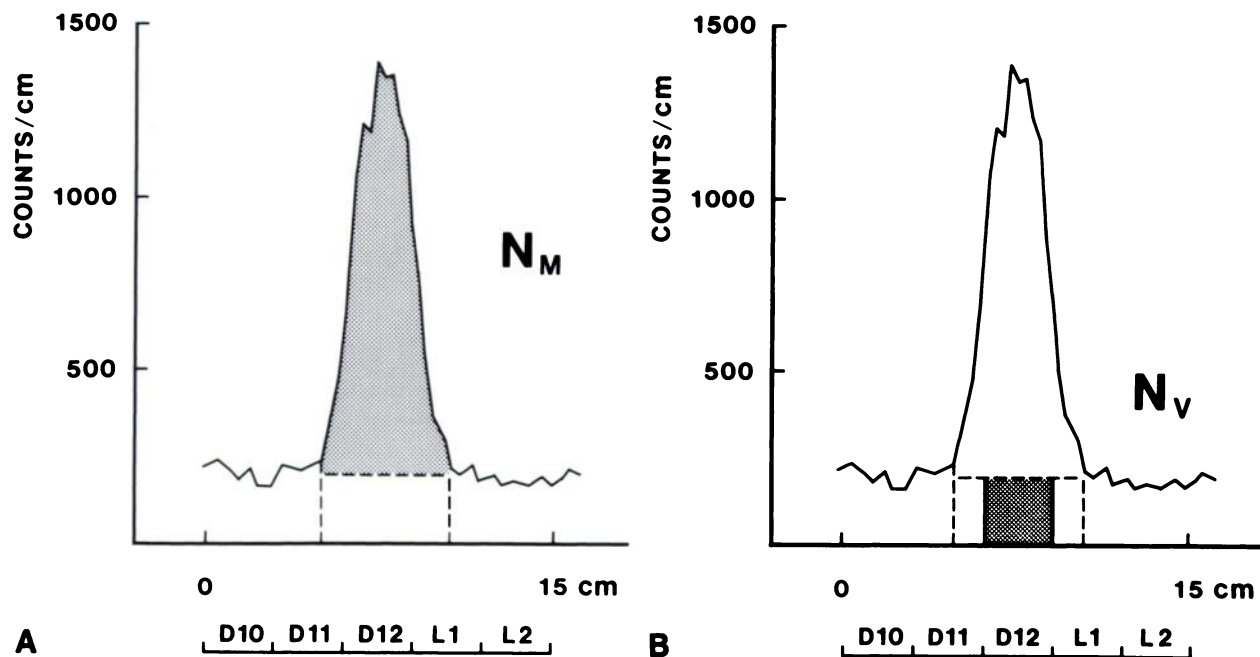


**FIGURE 2**

The vertical profile down the length of the spine derived from the posterior view  $^{85}\text{Sr}$  image of a patient with an isolated vertebral metastasis in D12. A: The shaded area (net counts  $N_M$ ) represents the metastatic counts after subtraction of the background derived from adjacent normal bone [Eq. (1)]. B: The shaded area (net counts  $N_V$ ) derived for the product of the mean count/cm for normal bone and the height of a single vertebra (3 cm), represents the counts from a normal vertebra.

Strontium-85 metastatic activity determined from Eq. (10) was decay corrected to the day of radiostrontium administration and expressed as a fraction of injected  $^{85}\text{Sr}$  activity. The conjugate view measurement of  $J_{\text{met}}$  was then used to normalize the complete set of decay corrected metastatic count rate data and obtain the curve of fractional metastatic strontium retention against time from 1 day to 6 mo after therapy.

#### Patients with Diffuse Vertebral Metastases

A rigorous determination of metastatic  $^{85}\text{Sr}$  uptake is also possible for the case of the patient with diffuse disease affecting all vertebrae in the field of view (Fig. 1B). The analysis is similar to that described above for the isolated metastasis, but with a modification in the way the set of ROIs is drawn. On posterior and anterior patient views, a set of ROIs is drawn with increasing width but a constant height equal to the height of a single vertebra (Fig. 1B). Under the assumption of uniform vertebral involvement, counts from the selected vertebra lost from the ROI due to the point response function of the gamma camera are matched by counts gained for the same reason from adjacent vertebrae. There is thus no net loss of counts across the horizontal lines that define the upper and lower edges of the ROI. The counts found for ROIs drawn in this manner are therefore equal to those that would be found for a hypothetical isolated single vertebra analyzed with ROIs that extend across the complete field of view in the vertical direction (Fig. 1C). The determination of vertebral metastatic activity proceeds as described above using Eq. (10), but differs in that no  $f_1$  correction is required, that posterior and anterior patient views are analyzed with the ROIs shown in Figure 1B, and the transmission, standard source and phantom images are analyzed with the ROIs shown in Figure 1C.

#### CT Imaging and Metastatic Mass

The prostatic vertebral metastases selected for dosimetric study consist of sclerotic trabeculae separated by intratrabecular cavities containing tumor cells and residual marrow. The scintigraphic measurements of strontium retention can be used to calculate the absorbed dose averaged over the entire metastasis provided the total mass of bone, tumor, and bone marrow involved can be measured. We used high resolution computed tomographic (CT) images to determine mass by, first, measuring the volume of the metastasis by drawing regions that defined the area of metastatic spread seen on sequential CT slices through the vertebra, and second, estimating the mean physical density of the metastasis from the mean Hounsfield number averaged over the volume of involved bone.

Volumes for the metastases being studied were obtained by imaging the patients with a Siemens DR2 whole-body scanner. After identification of the correct vertebra on a lateral scout image, the scanner gantry was aligned parallel with the disk space above the vertebra, and a continuous sequence of 4 mm width high resolution images obtained through the vertebral body. In all patients studied, the area of metastatic involvement was readily identified by its sclerotic appearance, and the CT images confirmed the impression of the [ $^{99m}\text{Tc}$ ]MDP study of complete involvement of the vertebral body. The area of tumor seen on each sequential CT slice was measured using standard ROI software provided by the manufacturer, the accuracy of which was checked by scanning phantoms of known cross sectional area. Typically, the sequence of images comprised five complete 4-mm slices through the middle of the vertebra with adjacent upper and lower slices through the cortical endplates. While the endplate slices appeared normal,

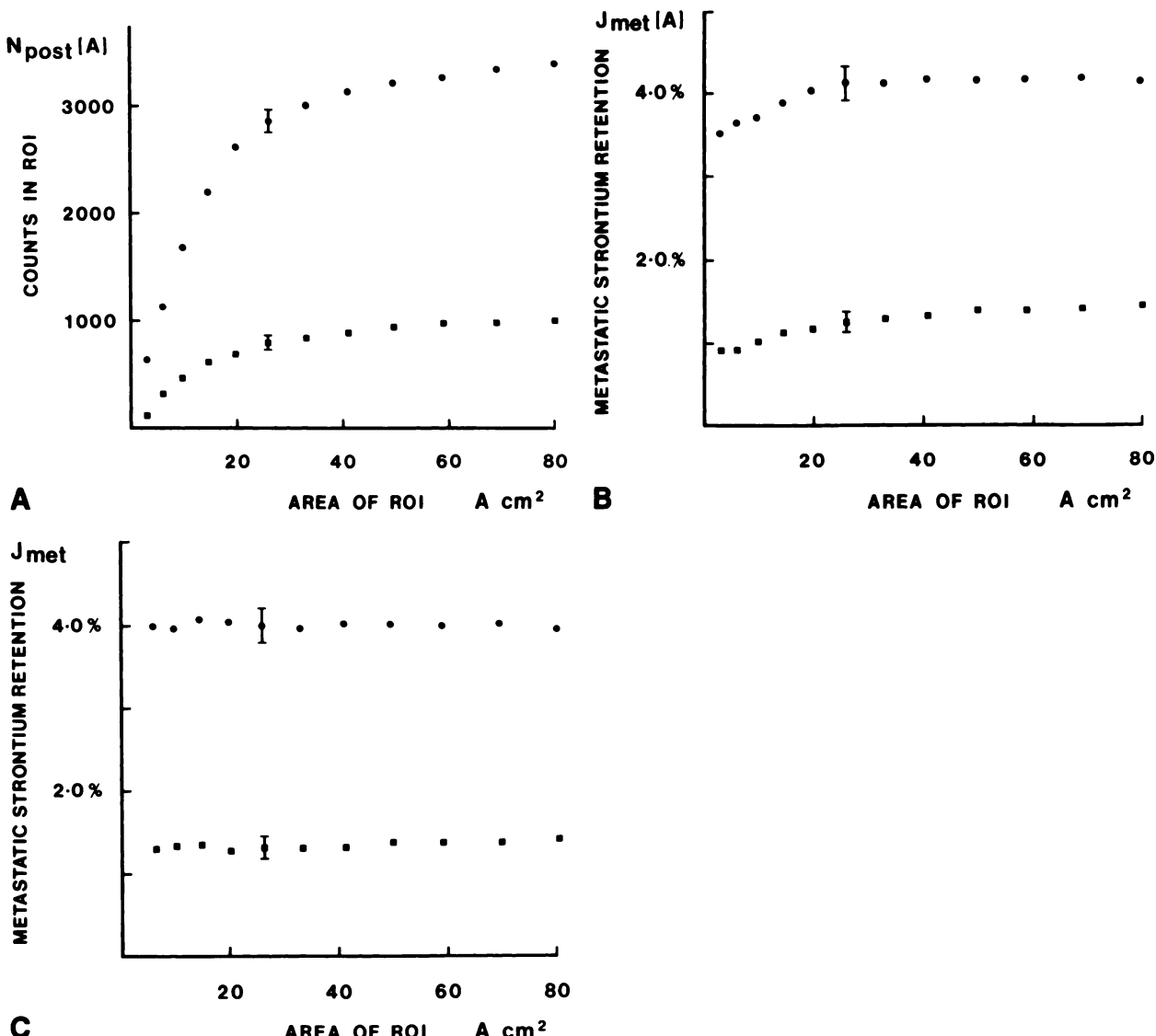


**FIGURE 3**

A:  $^{85}\text{Sr}$  counts within the set of metastatic ROIs superimposed on a posterior image,  $\tilde{N}_{\text{post}}(A)$ , as a function of the ROI area,  $A$ , for two vertebral metastases. Counts were corrected for the contribution of normal bone [Eq. (1)]. The error bars are  $\pm 2\sigma$ . B: Apparent metastatic strontium retention,  $J_{\text{met}}(A)$ , calculated from the conjugate view principle, as a function of ROI area.  $J_{\text{met}}(A)$  is expressed as a percentage of injected activity after decay correction. Curves shown are for the metastases in A. Note that  $J_{\text{met}}(A)$  varies with ROI area, albeit more slowly than  $\tilde{N}_{\text{post}}(A)$ . C: The true metastatic strontium retention,  $J_{\text{met}}$ , obtained by correcting the data of B from a conjugate view study of a phantom metastasis. After this correction, the variation of  $J_{\text{met}}$  with ROI area becomes smaller than the  $2\sigma$  statistical error.

they almost certainly included metastatic trabecular bone masked by the adjacent cortical bone. To avoid underestimating the true volume of involved bone, the following algorithm was used to determine tumor volume:

$$V = 0.4 \sum_{i=1}^n A_i + 0.5(A_{e1} + A_{e2})(h - 0.4n)\text{cm}^3, \quad (11)$$

where  $n$  is the number of slices through the middle of the vertebra,  $A_i$  the area on the  $i^{\text{th}}$  slice,  $A_{e1}$  and  $A_{e2}$  the areas on the endplate slices and  $h$  the distance between endplates determined from the lateral scout image.

The mean Hounsfield number over the volume of met-

astatic bone was obtained by averaging the mean CT number of each slice weighted by the area measured from the slice. Endplate slices were omitted to avoid biasing the result because of the high density of normal cortical bone in the latter. Bone density was calculated from Hounsfield units using the QCT calibration of Genant and Cann (15) in which the bone mineral content of vertebral trabecular bone is determined by standardizing the Hounsfield scale against a phantom containing solutions of dispatassium hydrogen phosphate ( $K_2\text{HPO}_4$ ) of known concentration. The Genant and Cann calibration was adapted to give the following relation between metastatic density and CT number, the derivation of which is given in

## Appendix 2:

$$\rho_{\text{met}} = 1 + \frac{(CT + 10)}{1250}. \quad (12)$$

Finally, metastatic mass was found by combining the volume measurement with that of mean density.

### Absorbed Dose to Metastases

Utilizing the complete set of metastatic strontium retention data for each patient, the time integral of the  $^{89}\text{Sr}$  activity curve was combined with the CT determination of bone mass to find mean absorbed dose using the following equation based on the dosimetric method of ICRP Publication 30 (16):

$$D_M = 1.6 \times 10^{-10} U_M \text{SEE}(M \leftarrow M) \text{ Gy}, \quad (13)$$

where  $D_M$  is the absorbed dose to the metastasis  $M$ ,  $U_M$  the total number of beta transformations occurring in  $M$ , and  $\text{SEE}(M \leftarrow M)$  the specific effective energy for  $M$ . For  $U_M$  we write:

$$U_M = A_\beta \int_0^\infty f_M(t) e^{-t/\tau} dt, \quad (14)$$

where  $A_\beta$  (units Bq) is the  $^{89}\text{Sr}$  activity initially administered to the patient,  $f_M(t)$  the fractional metastatic retention at time  $t$  (units s), and  $\tau$  the mean life of  $^{89}\text{Sr}$ . For specific effective energy we write:

$$\text{SEE}(M \leftarrow M) = \frac{E_\beta A F(M \leftarrow M)}{M_M} \text{ MeV g}^{-1}, \quad (15)$$

where  $E_\beta = 0.583$  MeV is the mean beta ray energy for  $^{89}\text{Sr}$  (17),  $A F(M \leftarrow M) = 1.0$  the absorbed fraction for beta rays originating in the metastasis, and  $M_M$  the mass (units g).

## RESULTS

The measured values of parameters involved in the dose calculation are summarized in Table 1, together with values of  $D_M$  inferred from Eq. (13). For three patients with diffuse metastatic disease (Table 1, Cases 8-10), their deterioration in health prevented us from obtaining  $^{85}\text{Sr}$  scintigraphy after 8 wk or CT images. However, the slow biologic elimination of  $^{89}\text{Sr}$  relative

to radioactive decay meant that there was little error in extrapolating the available data to estimate  $U_M$ . Dose was estimated by adopting a mass of 60 g on the assumption that, with increased involvement of spinous process and pedicles, metastatic volume was likely to be a little greater than in the patients with isolated metastases.

In a study of the relationship between  $^{89}\text{Sr}$  dosimetry and whole-body Sr kinetics, we discussed the significance of Sr renal plasma clearance and the extent of osteoblastic metastatic disease as factors influencing the absorbed dose delivered to skeletal metastases and showed how these effects may be modelled using impulse response function analysis (10). In Table 2, Sr renal clearances of the patients studied are listed together with a qualitative indication of the extent of skeletal metastatic disease demonstrated on  $[^{99m}\text{Tc}]$  MDP images. In Column 2, the dose measurements of Table 1 are expressed as absorbed dose per unit of administered  $^{89}\text{Sr}$  activity. In Column 5, we have calculated the doses that would have been achieved had the metastases been present in patients with the ICRP normal Sr plasma clearance of 10.4 l/day and negligible metastatic disease in the skeleton (10).

## DISCUSSION

For any small series of  $^{89}\text{Sr}$  therapy patients selected for dosimetric study, the findings will be partly determined by whole-body strontium kinetics in the particular subjects chosen. Our present results (Table 2, Column 2) show that the patients with isolated metastases and low values of Sr renal clearance (Cases 4-6) received doses two to three times larger than average, while for patients with extensive metastatic disease (Cases 7-10) dose was lower than average by a factor of 2 to 4. Our corrected doses allowing for these variables (Table 2, Column 5) show that the variations measured are consistent with those predicted by the impulse response function model (10).

**TABLE 1**  
Details of Dosimetric Calculations

Case no.	Vertebra studied	$^{89}\text{Sr}$ activity MBq (mCi)	$f_1$	disintegrations in metastasis $\times 10^{12}$	Metastatic volume $\text{cm}^3$	Metastatic density $\text{g/cm}^3$	Metastatic mass g	Absorbed dose Gy (rad)
1	L3	200 (5.4)	1.15	26	49	1.40	68	35 (3,500)
2	D12	189 (5.1)	1.20	23	35	1.44	51	42 (4,200)
3	D11	244 (6.6)	1.24	18	29	1.34	39	43 (4,300)
4	D12	185 (5.0)	1.19	39	35	1.44	51	71 (7,100)
5	L1	218 (5.9)	1.18	46	32	1.57	50	85 (8,500)
6	D11	226 (6.1)	1.07	52	26	1.37	35	138 (13,800)
7	L1	124 (3.4)	—	6	38	1.59	61	9 (900)
8	L1	99 (2.7)	—	9	—	—	(60)	14 (1,400)
9	L1	76 (2.1)	—	5	—	—	(60)	8 (800)
10	L1	126 (3.4)	—	5	—	—	(60)	8 (800)

**TABLE 2**  
Data Relevant to the Interpretation of Dosimetric Results of Table 1

Case no.	Absorbed dose per unit $^{89}\text{Sr}$ activity cGy/MBq (rad/mCi)	Sr renal plasma clearance 1/day	Extent of skeletal metastatic disease	Corrected absorbed dose <sup>a</sup> cGy/MBq (rad/mCi)
1	18 (670)	9.8	Light	21 (780)
2	22 (810)	3.5	Light	14 (520)
3	18 (670)	11.8	Light	22 (810)
4	38 (1,410)	0.1	Extensive	22 (810)
5	39 (1,440)	0.9	Moderate	18 (670)
6	61 (2,260)	1.8	Moderate	32 (1,180)
7	7 (260)	2.2	Diffuse	16 (590)
8	14 (520)	0.9	Diffuse	32 (1,180)
9	10 (370)	4.1	Diffuse	14 (520)
10	6 (220)	1.6	Diffuse	24 (890)

<sup>a</sup> Dosimetric data of Column 2 after correction for variations in Sr renal plasma clearance and extent of skeletal disease. Absorbed dose has been corrected to the dose that would have been attained in a subject with a net Sr plasma clearance of 10.4 1/day and minimal skeletal metastatic disease (10).

We have examined our dosimetric data in relation to clinical response to  $^{89}\text{Sr}$  therapy. The patients described here were part of a trial of radiostrontium therapy (5, 9) in which a detailed clinical assessment was made at 1, 2, 3, and 6 mo following therapy and patients scored for changes in bone pain, mobility, and analgesia. Of the three patients who received the highest absorbed dose (Table 1, Cases 4–6), two were classified as showing dramatic improvement, becoming pain-free without analgesic medication: one died pain-free after 5 mo, while the other remains pain-free at 9 mo. The third patient showed a favorable initial response, but relapsed after 1 mo with severe bone pain requiring external beam therapy. Of three patients receiving doses ~4,000 rad (40 Gy) (Table 1, Cases 1–3), all were classified as showing substantial response: one remains pain-free after 9 mo, while the other two required further  $^{89}\text{Sr}$  therapy after return of bone pain at 6 mo. The remaining four patients (Table 1, Cases 7–10) all had diffuse metastatic disease and received doses ~1,000 rad (10 Gy). Their advanced disease made follow-up and assessment of any benefit derived from radiostrontium therapy difficult: two died after 3 mo, and although one showed no benefit, the second showed substantial improvement in pain and mobility during the initial 6 wk following therapy. Another patient showed some response, but required retreatment when bone pain returned after 8 wk, while the final patient remains pain-free 4 mo after  $^{89}\text{Sr}$ . We hope to comment on the dose-response relationship in a later report when more data are available.

The objective of this report has been to describe a method of accurately estimating the dose to skeletal metastases during  $^{89}\text{Sr}$  therapy and to present our initial findings. We have discussed the difficulties resulting

from the choice of the metastatic ROI on the  $^{85}\text{Sr}$  images and described a way of analyzing images using phantom studies which reduces the uncertainty in metastatic uptake due to ROI selection to below the statistical counting error. The latter arises principally from limited counting statistics on anterior images and it varied between 3 and 5%. The small variations in the anterior and posterior depths of metastases from the depths chosen for the phantom studies were not a significant source of error in the phantom correction [Eq. (9)]. The sclerotic metastases of prostatic malignancy contrast sharply on CT images with the low density of normal trabecular bone making definition of tumor volume unambiguous, and we estimate that errors in volume measurement are no greater than 10%. Bone density for metastases can be estimated using an adaption of the QCT bone mineral calibration of Genant and Cann (15), and errors are probably no larger than 5%. The final errors in the tumor dose figures presented in Table 1 are believed to be ~20% for Cases 1 to 7, but larger for the other three cases for whom data were less complete.

The doses calculated in this report are mean doses averaged over the total mass of bone and soft tissue in the metastasis. The range of  $^{89}\text{Sr}$  beta rays in tissue is sufficient to ensure that, given a homogeneous distribution of strontium in bone, a uniform dose over bone and soft tissue in intratrabecular cavities may be assumed (18). However, the distribution of strontium within a metastasis may prove to be very inhomogeneous, and the consequences of this for tumor dose require further study.

To complement data on  $^{89}\text{Sr}$  tumor dose, an assessment of bone marrow dose is required. We recently described a method of estimating marrow dose in pa-

tients with minimal metastatic bone disease using  $^{85}\text{Sr}$  total-body retention data and reported ratios of tumor to bone marrow dose of around 10:1 for two of the patients discussed here (Table 1, Cases 1 and 2) (19). Theoretical studies suggest that the tumor to marrow dose ratio is unchanged by variations in Sr plasma clearance and extent of metastatic bone disease (10), and we believe the values measured in these two cases to be typical of the therapeutic ratio achieved during  $^{89}\text{Sr}$  therapy.

## ACKNOWLEDGMENT

The authors thank Amersham International for the gift of  $^{85}\text{Sr}$  and  $^{89}\text{Sr}$  strontium chloride.

## APPENDIX I

### Correction Factor $f_2$ in the Conjugate View Calculation [Eq. (4)]

The correction factor  $f_2$  introduced in the conjugate view calculation [Eq. (4)] allows for the finite distribution of activity in the metastasis along the anterior-posterior axis. To improve on the simple uniform slab estimation of  $f_2$  [Eq. (6)], the following numerical simulation was performed.

The set of CT images of each patient's vertebral metastasis was transferred to a VAX 11-730 computer for which software for multi-modality image processing has been developed (20). Each  $256 \times 256$  CT image was compressed to a  $64 \times 64$  array and then smoothed. Pixels with CT numbers  $<120$  were flagged as soft tissue and ascribed a physical density of  $(1 + \text{CT}/1024)$ . Pixels with CT numbers  $>120$  were flagged as bone and ascribed a density using Eq. (B7) in Appendix 2. The density array so obtained was used to calculate an array of linear attenuation coefficients assuming a mass attenuation coefficient of  $0.095 \text{ cm}^2/\text{g}$  for the  $514 \text{ keV}$  gamma ray of  $^{85}\text{Sr}$  (the small difference in the mass attenuation coefficients of soft tissue and compact bone was ignored). Three assumptions for the  $^{85}\text{Sr}$  activity distribution in bone were examined:

Model 1: activity per bone pixel constant

Model 2: activity per bone pixel proportional to bone density,  $\rho_{\text{bone}}$

Model 3: activity per bone pixel proportional to  $(\rho_{\text{bone}} - 1)$ .

The three models were chosen to study the effect of varying heterogeneity of metastatic  $^{85}\text{Sr}$  distribution on  $f_2$ . It was assumed that there was no  $^{85}\text{Sr}$  activity in soft tissue.

The accuracy of the conjugate view principle in determining the net metastatic  $^{85}\text{Sr}$  activity ascribed by the three models detailed above was examined by a numerical simulation in which the following quantities were evaluated: (i) the net activity summed over all bone pixels ( $J_{\text{bone}}$ ); (ii) the net activity weighted by the calculated attenuation factor for each pixel to the anterior edge of the image ( $J_{\text{ant}}$ ); (iii) the net activity weighted by the calculated attenuation factor for each pixel to the posterior edge of the image ( $J_{\text{post}}$ ); (iv) the mean anterior-posterior transmission factor through the metastasis ( $T$ ). The

correction factor  $f_2$  of Eq. (4) is defined by:

$$f_2 = \frac{\text{true activity}}{\text{conjugate view estimate}}. \quad (\text{A1})$$

From the numerical simulation described above, the value of  $f_2$  can be calculated by the relation:

$$f_2 = \frac{J_{\text{bone}}}{(J_{\text{ant}}J_{\text{post}}/T)^{1/2}}. \quad (\text{A2})$$

The mean values of  $f_2$  over the seven sets of CT images studied were:

Model 1:  $\bar{f}_2 = 0.977$  (range 0.971 – 0.983)

Model 2:  $\bar{f}_2 = 0.979$  (range 0.973 – 0.984)

Model 3:  $\bar{f}_2 = 0.984$  (range 0.977 – 0.987).

As the differences between patients and models are small compared with other errors in dosimetry, a value  $f_2 = 0.98$  was adopted for all patients.

## APPENDIX 2

### Derivation of Metastatic Density from Hounsfield Units

Let  $[\text{BMC}]$  be the bone mineral concentration expressed as mass of ashed bone per unit volume (volume here being the net volume of trabecular bone and intratrabecular cavities), and let  $[\text{K}_2\text{HPO}_4]$  be the concentration of aqueous dipotassium hydrogen phosphate solution with identical CT number. Both concentrations are expressed in units of  $\text{g}/\text{cm}^3$ . Genant et al. (15) obtained the following linear relationship:

$$[\text{BMC}] = 1.105[\text{K}_2\text{HPO}_4] + 0.0093. \quad (\text{B1})$$

Let  $\rho_{\text{bone}}$  be the density of the bone phase in the metastatic trabecular bone,  $\rho_{\text{soft}}$  the density of the marrow and tumour occupying the intratrabecular cavities, and  $w$  the ratio of ashed weight to live wet weight for bone. The mass of live wet bone per unit net volume is given by:

$$M_{\text{bone}} = \frac{[\text{BMC}]}{w} \quad (\text{B2})$$

and the fractional volume occupied by bone by:

$$V_{\text{bone}} = \frac{[\text{BMC}]}{w\rho_{\text{bone}}}.$$

Hence, the fractional volume occupied by tumour and marrow is

$$V_{\text{soft}} = 1 - V_{\text{bone}}$$

and its mass per unit net volume is given by:

$$M_{\text{soft}} = \left(1 - \frac{[\text{BMC}]}{w\rho_{\text{bone}}}\right) \rho_{\text{soft}}. \quad (\text{B3})$$

Combining Eqs. (B2) and (B3), the net mass of bone and soft tissue per unit volume gives the mean density of the metastasis:

$$\rho_{\text{met}} = \rho_{\text{soft}} + \frac{[\text{BMC}]}{w} \left(1 - \frac{\rho_{\text{soft}}}{\rho_{\text{bone}}}\right). \quad (\text{B4})$$

From ICRP Publication 23 (21), we adopted the following values:  $w = 0.54$ ,  $\rho_{\text{soft}} = 1.0$ ,  $\rho_{\text{bone}} = 2.0$ , giving:

$$\rho_{\text{met}} = 1 + \frac{[\text{BMC}]}{1.08}. \quad (\text{B5})$$

Solutions of known concentration of  $\text{K}_2\text{HPO}_4$  were made up in distilled water and scanned in a large volume water phantom, and the following linear relationship between  $[\text{K}_2\text{HPO}_4]$  and CT number obtained:

$$\text{CT} = 1280[\text{K}_2\text{HPO}_4]. \quad (\text{B6})$$

Eqs. (B1), (B5) and (B6) lead to the following relationship between CT number and the density of a metastasis:

$$\rho_{\text{met}} = 1 + \frac{(\text{CT} + 10)}{1250}. \quad (\text{B7})$$

## REFERENCES

1. Pecher C. Biological investigations with radioactive calcium and strontium: preliminary report on the use of radioactive strontium in the treatment of bone cancer. *Pharmacology* 1942; 11:117–149.
2. Firusian N, Mellin P, Schmidt CG. Results of strontium-89 therapy in patients with carcinoma of the prostate and incurable pain from bone metastases: a preliminary report. *J Urol* 1976; 116:764–768.
3. Silberstein EB, Williams C. Strontium-89 therapy for the pain of osseous metastases. *J Nucl Med* 1985; 26:345–348.
4. Robinson RG. Radionuclides for the alleviation of bone pain in advanced malignancy. *Clin Oncol* 1986; 5:39–49.
5. McEwan AJ, Zivanovic MA, Blake GM, et al. Sr-89 Therapy: clinical response in metastatic bone disease [Abstract]. *Nucl Med Commun* 1986; 7:293.
6. Maxon HR, Deutsch E, Libson K, et al.  $^{186}\text{Re}(\text{Sn})\text{HEDP}$ : a new agent for diagnosis and treatment of metastatic carcinoma to bone [Abstract]. *J Nucl Med* 1986; 27:948.
7. Eisenhut M, Berberich R, Kimmig B, et al. Iodine-131 labeled diphosphonates for palliative treatment of bone metastases: II. Preliminary clinical results with iodine-131 BDP3. *J Nucl Med* 1986; 27:1255–1261.
8. Goeckeler WF, Edwards B, Volkert WA, et al. Skeletal localization of Samarium-153 chelates: potential therapeutic bone agents. *J Nucl Med* 1987; 28:495–504.
9. Laing AH. Strontium-89 therapy for skeletal metastases [Abstract]. *Br J Radiol* 1987; 60:732.
10. Blake GM, Gray JM, Zivanovic MA, et al. Strontium-89 radionuclide therapy: a dosimetric study using impulse response function analysis. *Br J Radiol* 1987; 60:685–692.
11. Thomas SR, Maxon HR, Kereiakes JG. In vivo quantitation of lesion radioactivity using external counting methods. *Med Phys* 1976; 3:253–255.
12. Fleming JS. A technique for the absolute measurement of activity using a gamma camera and computer. *Phys Med Biol* 1979; 24:176–180.
13. Grossman LW, Fernandez-Ulloa M, Lukes SJ, et al. Gallium-67 lung uptake: conjugate-view technique. *Radiology* 1985; 157:789–793.
14. Jones DEA, Raine HC. Letter to the editor. *Br J Radiol* 1949; 22:549–550.
15. Genant HK, Cann CE, Ettinger B, et al. Quantitative computed tomography for spinal mineral assessment: current status. *J Comput Assist Tomogr* 1985; 9:602–604.
16. ICRP: Dosimetric model for bone. In ICRP Publication 30: Limits for intakes of radionuclides by workers. Part 1. Oxford: Pergamon Press, 1979: 35–46.
17. Cross WG, Ing H, Freedman N. A short atlas of beta-ray spectra. *Phys Med Biol* 1983; 28:1251–1260.
18. Whitwell JR, Spiers FW. Calculated beta-ray dose factors for trabecular bone. *Phys Med Biol* 1976; 21:16–38.
19. Blake GM, Zivanovic MA, McEwan AJ, et al.  $^{89}\text{Sr}$  radionuclide therapy:-dosimetry and haematological toxicity in two patients with metastasising prostatic carcinoma. *Eur J Nucl Med* 1987; 13:41–46.
20. Fleming JS, Britten AJ, Blake GM, et al. A general software system for the handling of medical images [Abstract]. *Nucl Med Commun* 1987; 8:270.
21. ICRP Publication 23: Report of the task group on reference man. Oxford: Pergamon Press, 1975.